Chapter 29

Characterizing Nanoscale Morphologic and Mechanical Properties of α-Synuclein Amyloid Fibrils with Atomic Force Microscopy

Kim K.M. Sweers, Martin Stöckl, Martin L. Bennink and Vinod Subramaniam

Nanobiophysics, MESA & Institute for Nanotechnology and MIRA Institute for Biomedical Technology and Technical Medicine, University of Twente, Enschede, The Netherlands

Chapter Outline

INTRODUCTION

α-Synuclein (aS) is a small protein implicated in the development of Parkinson's disease (PD) and is found abundantly in the human brain [1,2]. Recently, evidence was found that aS might be involved in regulating the size of synaptic vesicle pools [3–5]. One observation which leads to the hypothesis that the aggregation of aS is related to the development of PD is that there are three disease-related point mutations in the protein, A30P [6], E46K [7], and A53T [8], all of which have an impact on aggregation and fibrillization [9–13]. However, all disease-related mutants bind to phospholipid vesicles with a higher affinity to anionic lipids because of the positive net charge of the N-terminal region. A30P has a lower affinity for lipid vesicles when compared to the wild-type and the other two aS mutants because of the mutation in the N-terminus, which causes local disorder in the α-helix [14–17].

During disease progression, aS initially forms soluble oligomers which eventually self-assemble into amyloid fibrils in which the protein adopts a cross-β structure – a structure in which the β-strands are oriented perpendicular to the fibril's axis [18,19]. These fibrils accumulate in cytosolic inclusions, called Lewy bodies, which are the pathologic hallmark of PD [20–23]. As fibrils and prefibrillar oligomers seem to be the toxic species causing neuronal loss in PD, the characterization of fibrils of wild-type aS or the PD-related variants may yield valuable insight into processes involved in surface interactions and mechanical stability [24,25].

Atomic force microscopy (AFM) has proven to be ideally suited to investigate the nanoscale properties of these amyloid fibrils. In previous studies we have studied extensively the morphology of the aS fibrils, mainly focused on differences in the height of the fibrils, and the periodicity of height modulation along the length of the fibrils [26,27]. From these and other detailed AFM studies of amyloid fibril morphologies, structural models of amyloid fibril structure and assembly have been developed [28,29]. In order to get AFM images of amyloid fibrils representative of the fibril structure in solution, and extract accurate nanoscale properties, a proper choice of the underlying substrate is essential. The surface is obviously needed to attach and support the fibrils in order to enable AFM imaging, but the interaction of the surface with the fibrils must be such that the structure and the conformation of the fibrils are not influenced or altered.

Bio-nanoimaging. http://dx.doi.org/10.1016/B978-0-12-394431-3.00029-8

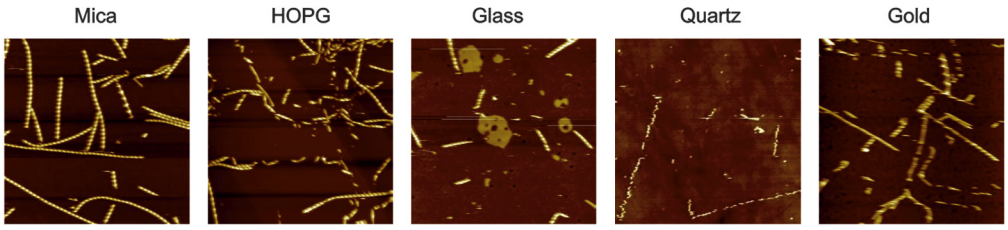

Height (nm)	7.9 ± 0.4	7.6 ± 0.6	8.7 ± 0.4	n/a	7.7 ± 0.5
Periodicity (nm)	40 ± 2	44 ± 4	42 ± 4	n/a	45 ± 3
Length (μm)	0.56 ± 0.37	0.25 ± 0.13	0.51 ± 0.34	n/a	0.56 ± 0.36

FIGURE 29.1 Tapping-mode AFM topography images of E46K fibrils deposited on five different substrates.

We report here a quantitative assessment of the nanoscale morphologic and mechanical properties of aS fibrils formed from the wild-type and three disease mutant proteins on various surfaces. Initially, we studied E46K disease-mutant fibrils deposited on mica, HOPG, glass, quartz and gold. Differences in apparent adhesion to the surface, as well as the average length of the fibrils, were observed to depend on the supporting substrate. As a next step, we studied the morphology of the wild-type and three disease-mutant aS fibrils on two different supported bilayer surfaces. The motivation to study these lipid bilayer surfaces is two-fold. First, the bilayer is considered as a more physiologically relevant surface for the amyloid fibrils, and second, the interaction between fibrils and lipid bilayers is thought to be a key factor in modulating cellular toxicity. We observed that, in contrast to monomeric aS, the fibrils do bind to the zwitterionic lipid (POPC) bilayer. We found that the fibrils formed with the disease mutant A30P had less affinity for the POPC lipid membranes, as inferred from the lower density of fibrils per unit area. All fibril samples formed large film-like patches of fibrils on the membrane, clearly indicating an attraction between individual fibrils. The absence of movement of the fibrils on the POPC–POPG lipid bilayer, combined with the ~3 nm lower height measured on this bilayer, suggests that the fibrils are incorporated in the membrane.

aS FIBRILS ON DIFFERENT SOLID SURFACES

Most reported AFM studies of amyloid fibrils, including aS, are carried out on a mica surface [26–28,30]. In most cases it is assumed that mica does not affect the conformation and structure of amyloid fibrils when they are deposited on the surface. Hoyer et al have shown – using *in situ* AFM – that, during fibril growth on a mica substrate, the underlying crystal structure of the mica can serve to template amyloid growth [31]. To validate the assumption that the substrate does not affect fibril structure, we deposited 50 μL of fibril solution on mica, HOPG, glass, quartz and gold substrates. After leaving the E46K aS fibrils on the surface for 1 hour, the surface was rinsed with 200 μL buffer, and subsequently 50 μL buffer was added to allow imaging in liquid.

Tapping-mode topography images of the aS fibrils are shown in Figure 29.1.

From the AFM images, the heights, lengths and periodicities of each fibril were determined with a custom written script in Matlab using the DIPimage toolbox (version 2.3, TU Delft, Delft, The Netherlands). The means and standard deviations of these fibril characteristics, measured for ~100 fibrils for each substrate, are presented in Figure 29.1. Each of the five surfaces was prepared in the same way, that is, exposed to 50 μL fibril solution derived from the same stock solution for an hour, after which it was rinsed. The density of aS fibrils on the surface is thus a relative measure of the affinity of these fibrils to the surface. For both mica and HOPG this surface coverage is relatively high (7.1 and 10.5 fibrils per μm^2) [30]. For the gold surface, this affinity is four times lower, and for glass and quartz the density, and thus affinity, is more than 10 times lower. The heights and periodicities of the fibrils are relatively similar, except that on glass the fibrils appear to be roughly 1 nm higher, most probably due to a difference in the interaction of the tip with the remaining surface [32]. When deposited on HOPG, the fibrils do have an average length that is about half that of those deposited on mica, glass or gold. This suggests that the interaction of the fibril with HOPG likely influences its structure, an observation that has been made with other biologic molecules and fibrillar structures deposited on HOPG [33,34]. Deposition on quartz appears to severely affect the structure of the fibrils. The density of fibril fragments that attach is very low, but, most importantly, the fibrils appear to be fragmented, most likely due to their interaction with the quartz substrate. The similar heights, lengths and periodicities demonstrated by the fibrils deposited on mica, glass and gold suggest that mica (and the other two substrates) do not significantly influence the fibril morphology as it is present in solution.

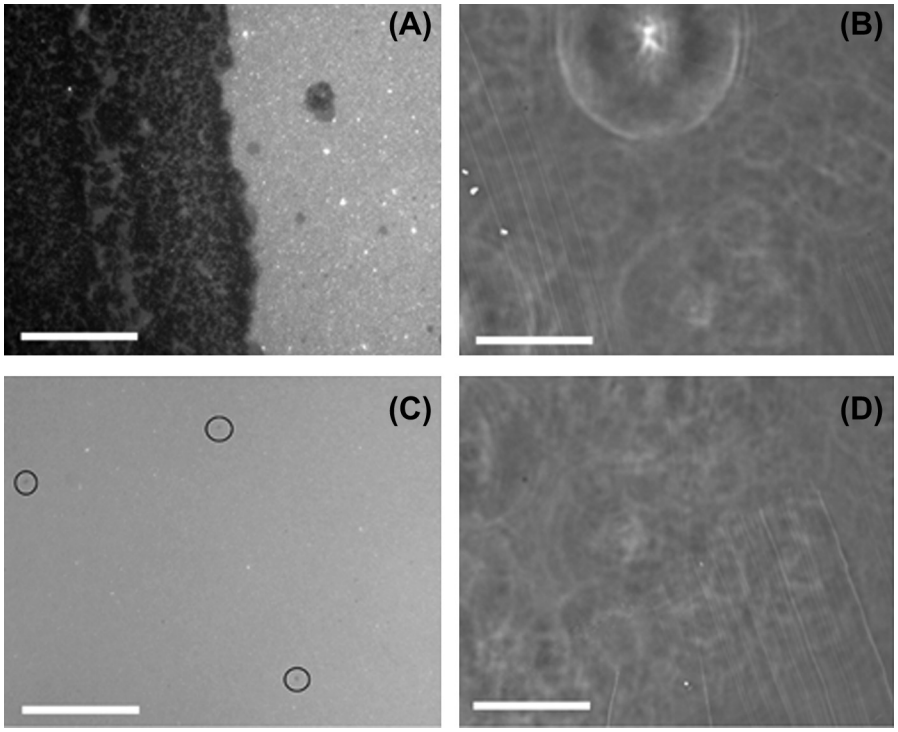

FIGURE 29.2 Fluorescence and corresponding light microscopy images of the POPC bilayer on mica. The layer contains 1% fraction DOPE labeled with rhodamine. (A) Fluorescence microscopy image clearly shows the transition from mica (*left*) to the lipid bilayer (*right*), where, in the corresponding white light image (B), no transition is to be seen. (C) shows a uniform fluorescent POPC bilayer (with corresponding white light image (D)) with three small defects (black circles). Scale bars are 100 μm. Images were recorded using a 40× objective on a Nikon Eclipse TE-2000-U (Nikon Corporation, Tokyo, Japan). Rhodamine fluorescence was excited at 530±20 nm and recorded at 617±36.5 nm (dichroic mirror cut-off at 562 nm).

PREPARATION OF SUPPORTED LIPID BILAYERS ON MICA

To prepare the supported lipid bilayers, we have used 1-palmitoyl-2-oleoyl phosphatidylcholine (POPC) and 1-palmitoyl-2-oleoyl phosphatidylglycerol (POPG) stock solutions in chloroform (Avanti Polar Lipids Inc, Alabaster AL, USA). In this study we have made 100% POPC bilayers, and a mixed bilayer consisting of 65% POPC and 35% POPG. The first step is to make a solution of lipid vesicles. By drying the phospholipid solution under a stream of nitrogen in a glass vial, a thin lipid film was formed. The POPC films were rehydrated in 10 mM Tris-HCl buffer with 150 mM KCl, pH 7.4, and the POPC–POPG mixture film was rehydrated in 50 mM NaCl, both to yield a total lipid concentration of 1 mM. In a next step, large unilamellar vesicles were prepared by extruding this vesicle solution eleven times through a 100 nm polycarbonate membrane filter (Isopore™ Membrane Filters, Millipore, Billerica MA, USA).

For preparing the supported bilayer on mica, 200 μL of the vesicle solution was deposited on freshly cleaved mica and was left to adsorb for 30 minutes. In the case of the mixed POPC–POPG vesicles, the ion concentration was increased from 50 mM to 1 M NaCl immediately after deposition on the freshly cleaved mica surface. Subsequently, the substrate was gently washed with fresh 50 mM NaCl buffer to remove any remaining vesicles in solution.

The unilamellar POPC vesicles that were attached to the mica surface fused to form a flat uniform supported lipid bilayer, which remained fluidic. This was verified by scratching the bilayer with the AFM tip and imaging the self-repairing capability of the bilayer. After scratching the surface with a considerable force we did not observe the scratch when imaging the same area subsequently. The uniformity of the layer on mica was also verified on a larger length scale using fluorescence microscopy (Figure 29.2). For this sample the POPC was mixed with 1% rhodamine-labeled DOPE.

AFM imaging of the supported POPC bilayer revealed small lipid patches on top of the bilayer (few hundreds of nanometers in size), but otherwise the layer was uniform. These lipid patches were typically around 4 nm in height (Figure 29.3). In contrast, the POPC-POPG membrane had multiple layers. From the height differences the thickness of these layers was found to be ~4 nm corresponding to the thickness of lipid bilayers and not monolayers. Due to the fluidity and self-repairing capabilities of the membrane it was not possible to measure the height of the uniform lipid layer by AFM.

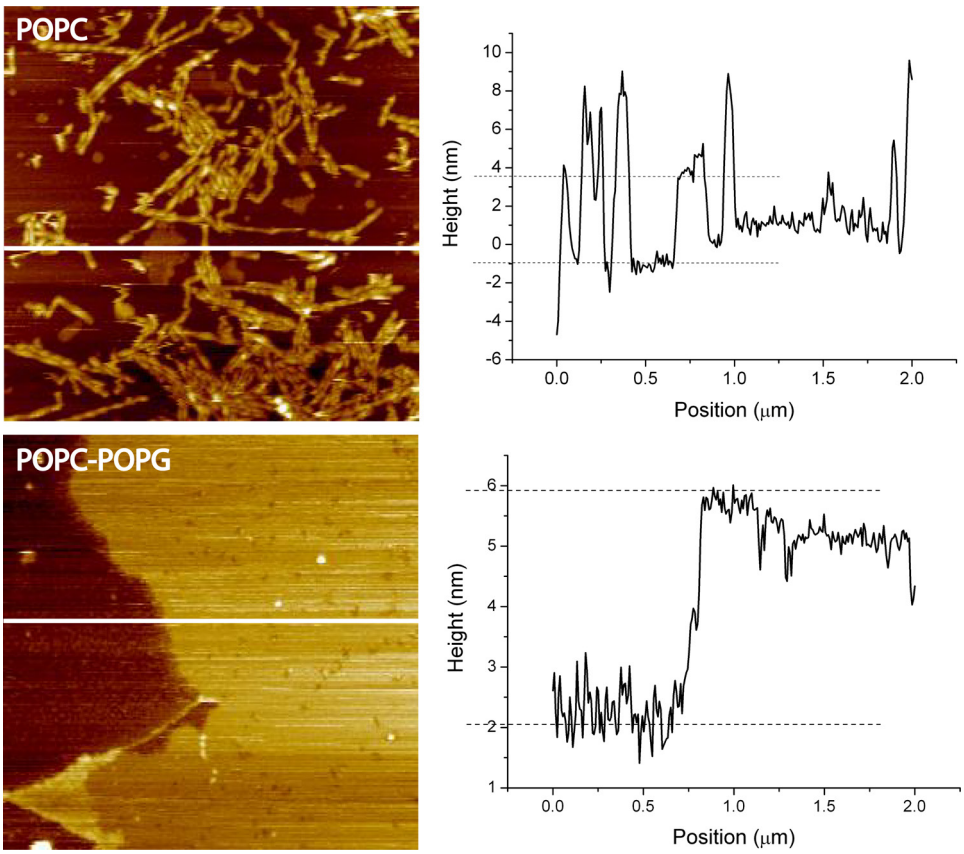

FIGURE 29.3 (*Top*) Topography image of aS fibril on supported POPC bilayer, showing occasionally small patches. From the line section it is clear that they are 4–5 nm in height. (*Bottom*) Topography image of the supported POPC–POPG bilayer (no fibrils), clearly showing that large multilayered parts were found. Height differences between the different layers are about 4–5 nm, suggesting that they are bilayers.

α-SYNUCLEIN MONOMERS ON SUPPORTED BILAYERS

The interaction of aS with lipid membranes plays an important role in the exertion of the physiologic function of the protein when bound to synaptic vesicles. For that reason, the binding of aS to lipid vesicles composed of different lipids and various sizes has been studied previously. In these studies the lipid bilayers always exhibited a curvature due to the spherical shape of the vesicles. To verify that the binding behavior of aS monomers is unaltered for flat supported lipid bilayers, we have added monomeric aS in the surrounding medium while imaging the POPC and POPC–POPG membrane continuously for at least an hour.

At t = 0, a solution of monomeric aS is injected, resulting in a final protein concentration of 30 μM. The AFM height images recorded at different time intervals are displayed in Figure 29.4. There is no significant aS monomer adsorption observed for the POPC layer, while protein monomers are seen to adsorb readily onto the POPC–POPG bilayer (65% POPC and 35% POPG in molar ratios), which is consistent with literature reports [16,35–37]. This corroborates that monomeric aS does not show affinity for membranes solely composed of zwitterionic lipids, but does exhibit affinity for negatively charged lipids. The adsorption on the mixed POPC–POPG bilayer is a very rapid process because protein nanostructures are already present on the membrane at time point zero. The adsorption of monomers seems to occur within 30 minutes because the image at t = 60 minutes reveals a similar density of attached protein monomers compared to the image at t = 30 minutes.

α-SYNUCLEIN FIBRILS ON POPC-SUPPORTED BILAYERS

aS fibrils are the main constituents in the Lewy Bodies associated with advanced stages of PD [20–23]. As the length of these fibrils is comparable to the diameter of mammalian cells, it is reasonable to assume that the accumulation of fibrils has consequences for interactions with the cell cytoskeleton and other cellular components, leading to changes in the mechanical properties of the cells. It is thus of great interest to characterize fibril mechanical properties, such as their flexibility, which is expressed as the persistence length. In order to measure this flexibility correctly, it is essential to know how the fibril is deposited on the substrate. The mode of deposition determines how the observed curvature (in the 2D AFM image) of the protein fibril is related to its flexibility

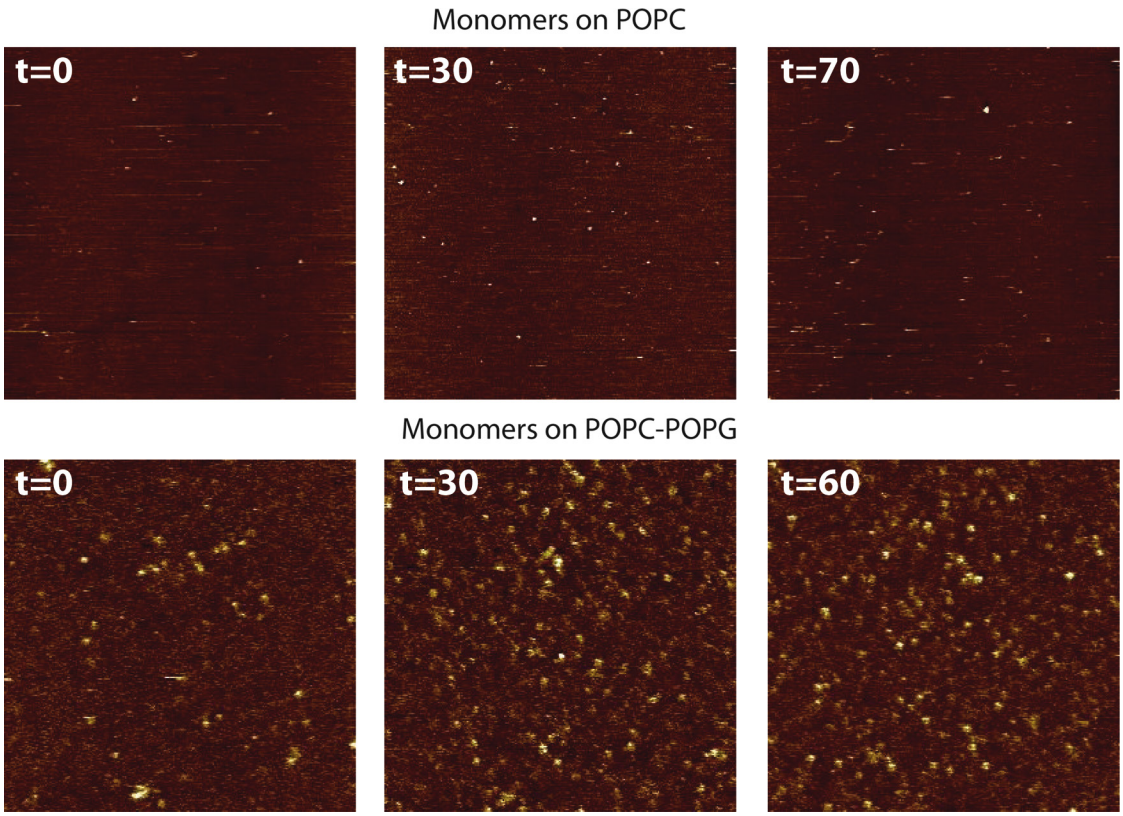

FIGURE 29.4 AFM height images of wild-type aS on POPC (*top row*) and POPC–POPG supported lipid bilayers at different times after addition of the protein (*bottom row*). Image size is 2×2 μm for all images and the z-range is 2 nm for the upper row and 5 nm for the lower row.

in solution. In all studies determining the persistence length of amyloid fibrils from AFM images it is implicitly assumed that, before the fibrils firmly attach to the surface, the amyloid fibril is able to equilibrate on the 2D surface. If this deposition model is correct, the curvature observed in the AFM images is indeed the curvature the fibril has when free in solution, and subsequently its persistence length can be readily determined using the appropriate methods. If, due to strong interaction forces, the fibril is pulled towards the surface without having a chance to equilibrate, this does not hold, and it becomes more difficult to unequivocally determine its persistence length.

We started out by studying aS fibrils deposited on supported lipid bilayers formed by POPC, as these membranes have been demonstrated to remain fluidic when formed on a mica substrate because of the thin water layer trapped between the mica and the membrane [38]. The fluidity of the membrane, combined with the low affinity of aS for POPC membranes, is expected to allow fibril movement on the substrate [16,35–37]. Under these conditions it is expected that the fibrils are thermally equilibrated on the surface before adhering more strongly, without having to consider any trapping effects [39].

In strong contrast to aS fibrils on mica, in which the fibrils are firmly attached, consecutively recorded AFM images of these fibrils on the POPC substrate demonstrated that the fibrils adsorb on membrane POPC bilayer, yet are still able to move around (Fig. 29.5). This may be due to the relatively weak interaction of the fibrils with the POPC bilayer, but may also be caused by the fluidity of the lipid layer itself. Fibrils in the topography images appear somewhat fragmented, which is probably an artifact of the scanning. Due to the weak interaction between the fibrils and lipids, or the lipids and the underlying substrate, the AFM tip was able to push the fibrils back and forth as it is scanning across the surface. This is corroborated by the observation that fibrils which appear fragmented in one image may appear intact in a consecutive scan. Some images furthermore show horizontal stripes because of the fluidity of the membrane. This effect can also be seen in Figure 29.4 for POPC only bilayers.

In order to characterize the impact, if any, on fibril adhesion to the substrate of the point mutations associated with hereditary forms of PD, for each aS variant AFM topography images were recorded in air (images not shown), in liquid on mica, and in liquid on the POPC-supported bilayer to systematically analyze fibril characteristics in different environments and on different surfaces. On the POPC bilayer, 40 AFM images were recorded for every variant to determine the affinity of the four variants to POPC. Wild-type fibrils and the E46K mutant fibrils on the POPC layer showed no clear differences in number of fibrils. The same number of fibrils (little over 70 fibrils, see also Table 29.1)

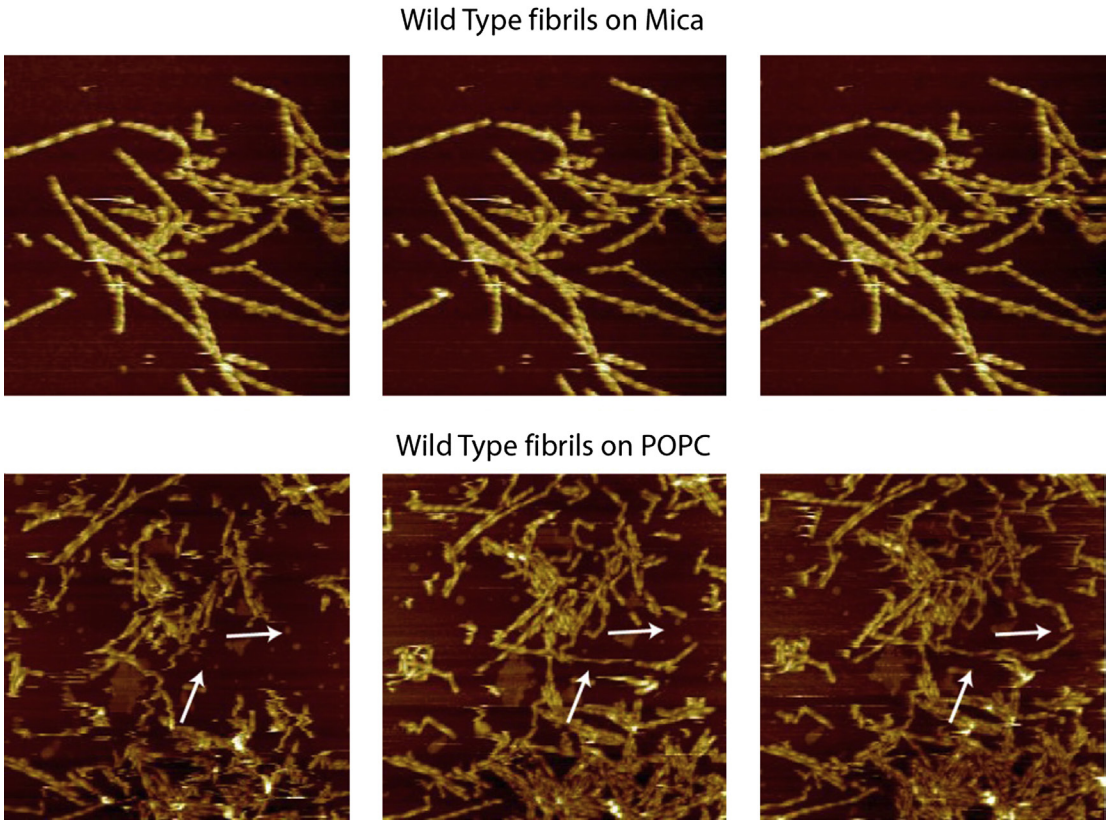

FIGURE 29.5 Consecutively recorded AFM height images of wild-type fibrils on mica (*upper row*) and on the POPC supported bilayer (*lower row*). On the mica surface the fibrils appear intact and fixed onto the surface. On POPC the fibrils appear fragmented and loosely bound to the surface. They are able to move around, as indicated by the white arrows. AFM images were made in aqueous buffer, scan size 2×2 μm, z-range 17 nm.

TABLE 29.1 Fibril Heights of α-Synuclein Variants

	Mica (in air)		Mica (in liquid)		POPC (in liquid)		Density (on POPC)
	Height[a] (nm)	N	Height (nm)	N	Height (nm)	N	Nr per 1000 μm^2
Wild-type	9.0 ± 1.2	42	9.3 ± 1.1	70	8.4 ± 0.8	76	76
E46K	8.0 ± 0.8	30	8.4 ± 0.9	51	6.2 ± 1.2	77	77
A30P	7.9 ± 0.7	62	9.0 ± 0.4	48	6.7 ± 0.9	21	21
A53T	8.8 ± 0.9	60	9.1 ± 1.0	49	8.7 ± 0.7	70	70[b]

[a]Fibril heights of the four different aS variants (wild-type, E46K, A30P and A53T) measured on a mica substrate in air and liquid. The decrease in fibril height from liquid to air was between 10% and 20%. The last column shows the relative surface coverage expressed as number of fibrils heights on 1000 μm^2 POPC membrane in liquid conditions.
[b]For A53T a 10 times more concentrated protein solution was needed to observe the 70 fibrils on 40 images.

was found in 40 AFM images; these fibrils met the inclusion criteria of being longer than 1 μm and appeared not to be fragmented. However, the A30P mutant showed significantly less binding to the POPC substrate. Here, in 40 images. only 21 fibrils were found. Many of the A30P fibrils appear fragmented, which we attribute to a lower affinity to the POPC-bilayer, leading to a propensity for the fibrils to slip upon contact with the AFM tip during imaging. A53T fibrils showed even less affinity for the POPC substrate. We needed a 10 times higher concentrated protein fibril solution to observe a similar number of fibrils (namely, 70 fibrils, see Table 29.1) on the POPC surface. Typical AFM topography images are displayed in Figure 29.6.

Fibrils prepared from all four aS variants showed affinity for the POPC membrane; however, for A53T, we needed significantly more fibrils to get the same surface coverage

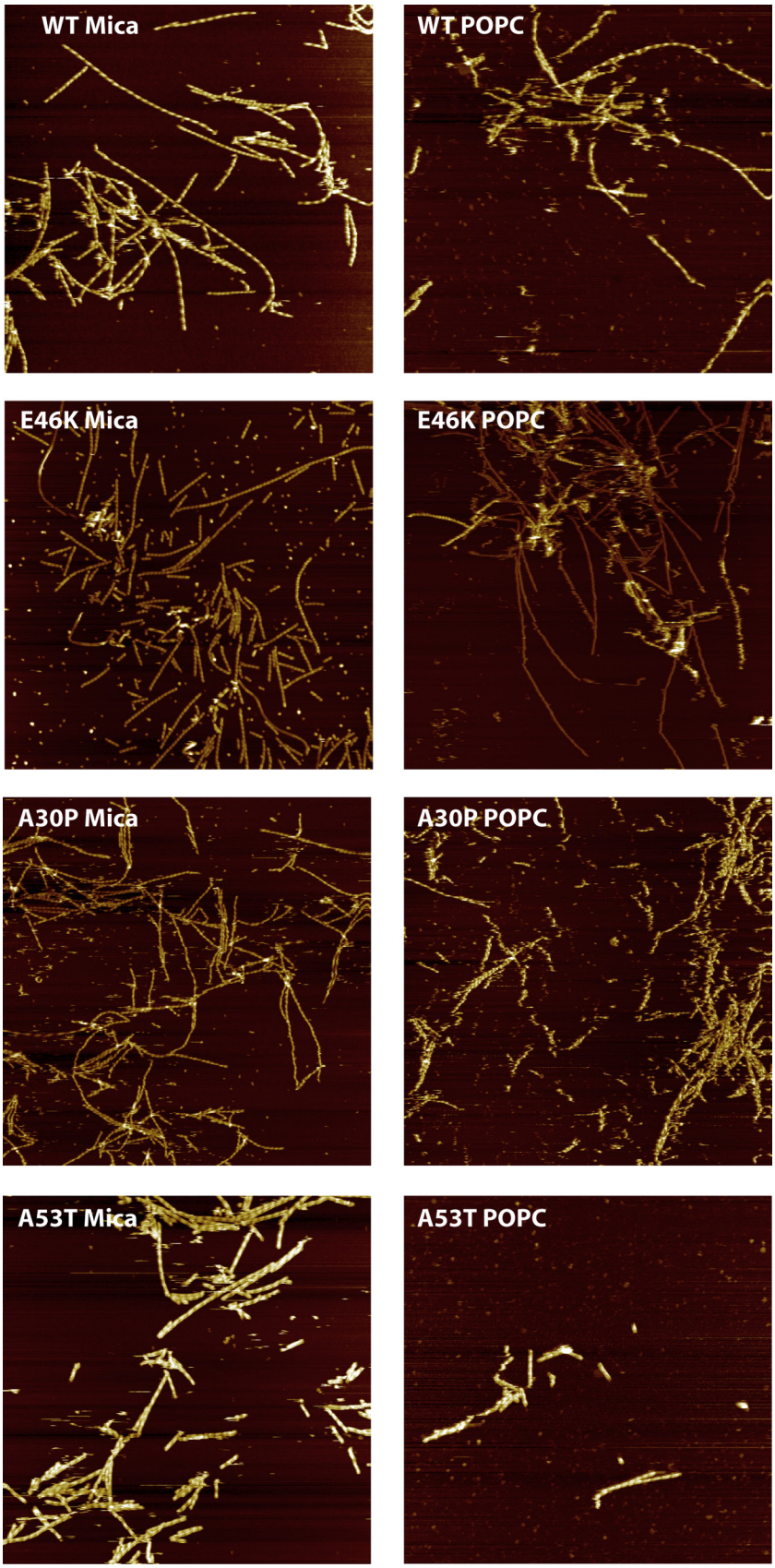

FIGURE 29.6 Typical AFM height images of fibrils made from wild-type and three different aS disease-related variants on mica substrate (*left column*) and POPC bilayer (*right column*). AFM images were recorded in aqueous buffer, scan size 5×5 μm, z-range 20 nm. For wild-type, E46K and A30P the same protein concentration is used, for A53T the sample was 10 times more concentrated compared to the other three variants (see also Table 29.1).

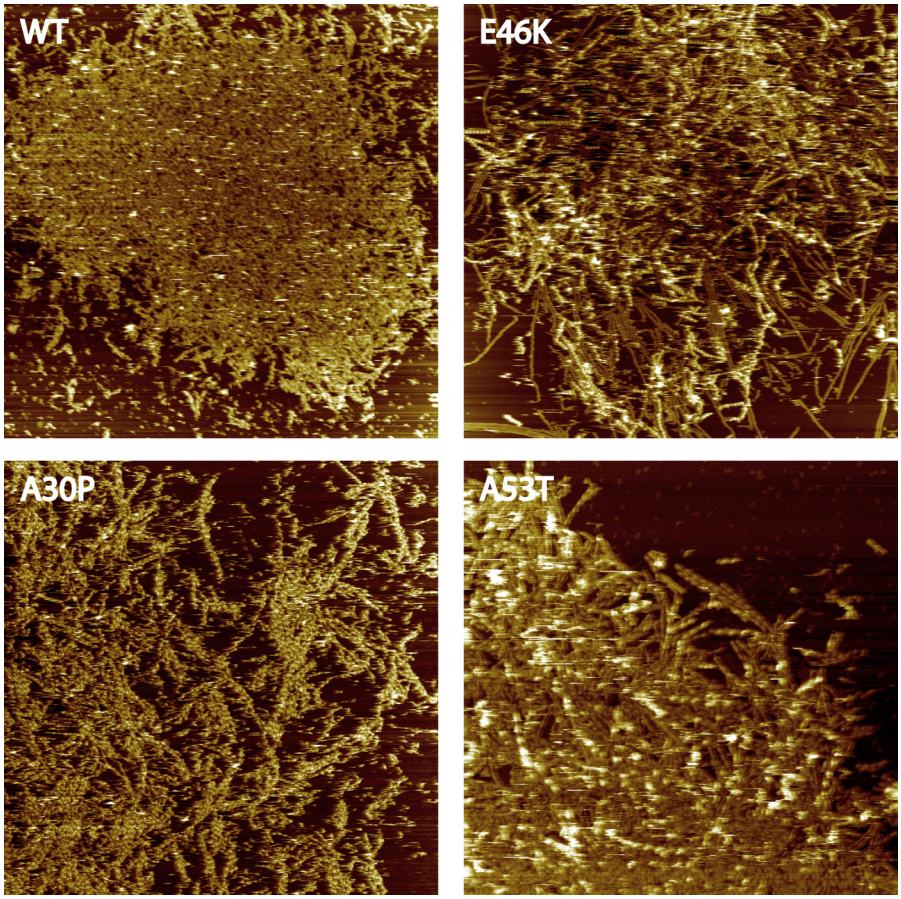

FIGURE 29.7 Clusters of aS fibrils found on the POPC bilayer, image size 5×5 μm, z-range 20 nm.

(2 times diluted compared to 10 or 20 times for the other variants). The binding to the membrane was, for all four variants, only loose, allowing for slippage during scanning as seen by the apparently fragmented fibrils observed on POPC bilayers. Just as in monomeric aS, A30P fibrils had a lower affinity for lipids when compared with the other three variants. This resulted in a lower number of fibrils on POPC bilayers for the analysis. This observation suggests that, also in fibrillar form, the structure of the N-terminus plays a role in lipid binding. The affinity of the wild-type fibrils for POPC–POPG is comparable to that for the POPC membrane (31 fibrils on 20 images compared to 76 fibrils on 40 images). However, all fibrils were firmly bound, that is, no fragmented fibrils were observed and all fibrils were considerably lower in height.

In some places on the surface, patch-like clusters of fibrils on the POPC membrane were found for the wild-type protein and the three mutants (Fig. 29.7). The ability of the fibrils to move on the lipid surface in combination with attractive fibril–fibril interactions most probably leads to the clustering of the fibrils. The clusters had heights similar to those measured on individual fibrils, indicating a monolayer of fibrils. The fluidity of the POPC membrane, either alone or combined with the low adsorption of the fibril to the membrane, most probably allows the fibrils to move around. This movement of the fibrils on the membrane created a monolayer of fibrils. This observation suggests that fibrils may cluster into higher ordered assemblies in close proximity of membranes. Clustering and alignment of protein fibrils on different kinds of surfaces has been seen previously [40].

The heights and periodicities of the fibrils were analyzed. Fibril heights were consistently higher when measured in liquid on mica as compared to the heights measured in ambient conditions (see Table 29.1). The heights of the fibrils on the supported membrane were consistently lower when compared to the heights obtained on mica for all fibril variants. This could suggest that the fibrils are somewhat incorporated in the membrane. Periodicities of the fibrils of all variants ranged from 65 to 140 nm. The periodicities of each fibril species did not change when measured on the different surfaces or under different environmental conditions.

Morphologic analysis of the fibrils on mica and on the POPC membrane showed no significant differences compared to previous studies [26,27,29,41]. Periodicities are

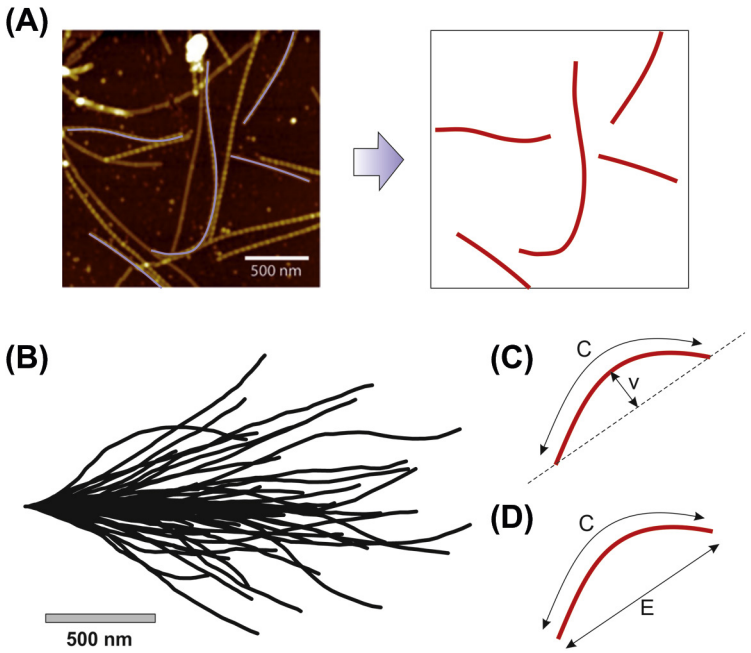

FIGURE 29.8 (A) Representative AFM topography image of E46K fibrils (*left*) and a set of contours (*right*) extracted from the image. (B) Complete set of contours extracted from a set of AFM images. (C,D) Schematic representations of how the curvature is analyzed by determining the deviation of the midpoint of the fibril segment from its secant line (C), and by determining the end-to-end distance (D).

slightly different compared to other studies; in particular, the E46K variant showed a larger periodicity (~70 nm) compared to the often-measured 45 nm. However, the aggregation conditions (70° Celsius and no extra ions) deviated from other studies [26,27,29], which might explain this difference. Recently, Adamcik et al showed periodicity differences for amyloid fibrils when aggregated or adsorbed on the surface with different ion concentrations [42]. Yet the fibril heights are comparable to previous studies; also, the height differences measured in liquid versus air (20%) have been observed previously [26,27,43,44]. There is a slight height difference between fibrils measured in liquid on mica compared to those on POPC bilayers. However, this height difference is below 1 nm, a difference that could also be attributed to the AFM settings, as, for instance, the force setpoint, or environmental conditions [32,43].

INFERRING THE MECHANICAL PROPERTIES OF FIBRILS FROM IMAGES

Determination of the mechanical properties of amyloid fibrils, such as the bending rigidity or persistence length, can be done by analyzing the contours of the fibrils as they appear in the AFM topography images. As a first step, a custom-written Matlab script has been used to isolate and trace the fibril contours (see Fig. 29.8A), which are at least 1 μm in length and do not cross other protein fibrils. The fibril contours are exported as arrays of x and y coordinates of the pixels making up the fibril. A collection of these contours representing aS fibrils is presented in Figure 29.8B. These data are then further analyzed using two different methods to get the persistence length of the fibrils (Fig. 29.8, C and D).

The first method measures the deviation of the fibril shape in AFM topography images from a secant line connecting its ends (Fig. 29.8C). The average of the squared value of this deviation, which is the variance of the distribution of the deviation itself, is directly related to the persistence length (Eq. 1).

$$P = \frac{C^3}{48\,\langle v^2\,(x)\rangle} \tag{1}$$

This method has been used for several amyloid fibrils, such as insulin fibrils [45], aS fibrils [44], and HypF-N fibrils [46]. This method is valid only for segments of length L that are much shorter than the persistence length of the fibril. If this is not the case, smaller parts of the contours can be taken and analyzed. For the analysis of the aS fibrils in this study we have analyzed segments of different lengths between 50 and 300 nm, and the average is taken of the persistence lengths determined for each length.

For the second method, the end-to-end distance and the contour length is determined for each fibril (Fig. 29.8D). After plotting the squared value of the end-to-end distance versus the contour length, the curve can be curve-fitted with Eq. 2 in order to determine the persistence length.

$$\langle E^2 \rangle_{2D} = 4PC\left(1 - \frac{2P}{C}\left(1 - e^{-\frac{C}{2P}}\right)\right) \tag{2}$$

TABLE 29.2 Persistence Lengths of α-Synuclein Fibrils

Fibril	Surface	P (method 1)	P (method 2)	N
Wild-type	Mica	8.1 ± 1.0 mm	3.9 ± 0.3 mm	70
	POPC	5.3 ± 1.4 mm	3.5 ± 0.3 mm	76
E46K	Mica	5.6 ± 0.8 mm	6.2 ± 0.5 mm	51
	POPC	6.1 ± 1.7 mm	11.9 ± 1.8 mm	77
A53T	Mica	7.1 ± 0.8 mm	6.9 ± 2.2 mm	49
	POPC	5.3 ± 1.0 mm	5.4 ± 0.8 mm	70
A30P	Mica	5.3 ± 0.8 mm	5.0 ± 1.3 mm	48
	POPC	3.4 ± 1.0 mm	3.3 ± 0.9 mm	21

This method has no limitation in the length of the contours used. We have analyzed for each fibril the end-to-end distance and contour length, resulting in one datapoint per fibril, but it is also possible to take shorter segments (parts of fibril) and perform the same analysis. This method has, for example, been applied for determining the persistence length of beta-lactoglobulin fibrils [42].

Both methods are based on the worm-like chain model and, as already mentioned earlier, the Eq 1 and 2 yield the correct persistence length only if the fibrils are in thermal equilibrium when adsorbing on the surface. This means that before attaching firmly to the surface, the amyloid fibril is able to equilibrate on the 2D surface, such that the curvature observed in the AFM height image is indeed the curvature it would have in its 3D conformation. If this condition is not completely fulfilled, and the fibril attaches directly from its 3D conformation onto the surface, and the appearance of the fibril on the surface is more or less the 2D projection of its 3D conformation, then the observed persistence length using the above methods is expected to be lower. Mucke et al [47] have shown that, when the 3D conformation is effectively flattened into a 2D conformation, the observed persistence length is half that of its real value.

In many cases, however, the mode of deposition onto the surface is not clear. Considering the mobility of the fibrils observed on the POPC monolayer, the fibrils are clearly able to move along the substrate, either because the adhesion of the fibril to the bilayer is not that strong, or because the lipids in the bilayer are free to move. These are the necessary conditions for the fibril to equilibrate in 2D, and thus can the persistence length be determined using the above equations.

Using both methods, the average persistence lengths of fibrils from the four protein variants, on mica and on the POPC bilayer, are analyzed (see Table 29.2). The persistence lengths found are within the range of 3.3 to 7.1 μm, which corresponds with a bending rigidity of 1.3 to 2.9 · 10^{-26} Nm^2. This is within the range of bending rigidities found for other amyloid structures [48].

Please note that the error given in the table is determined by the curve-fitting procedure. There is, however, another uncertainty that plays a role. In method 1, the accuracy in determining the persistence length is basically set by the uncertainty in the determination of $\langle v^2 \rangle$. What is important to realize is that v is Gaussian distributed around zero. $\langle v^2 \rangle$ in this context is then the variance of this Gaussian distribution. If more data points (N) are included in the distribution, the variance can be determined more accurately. In order to determine this accuracy, we have done some simulations. We have drawn N numbers from a normal distribution, and determined $\langle v^2 \rangle$ from these drawn numbers. If one does this 10^6 times, one can determine the accuracy with which the variance, and thus the persistence length, can be determined. The accuracy is calculated in percentages of the mean value. From this simple simulation it becomes directly clear that the accuracy increases as N increases. For N = 30 this uncertainty is about 30%, and for N = 100 this uncertainty is about 15% of the value. The uncertainty in method 2, using the end-to-end distance versus the contour length, is also determined by the variance of a distribution (this one is not Gaussian, and not centered around zero) and a similar simulation has been done to determine its accuracy. For N = 30 this is about 16%, and for N = 100 this uncertainty is about 9%.

The differences in persistence lengths measured on mica and POPC for the four aS mutant fibrils are quite small. For the wild-type and E46K, if both methods are taken into account, there is hardly any difference. For A53T and for A30P, the persistence length on POPC seems to be systematically slightly lower than when measured on mica (20% and 45% respectively). It is interesting to note that, based on the observation of fibril movement on POPC, we can conclude that the necessary conditions for

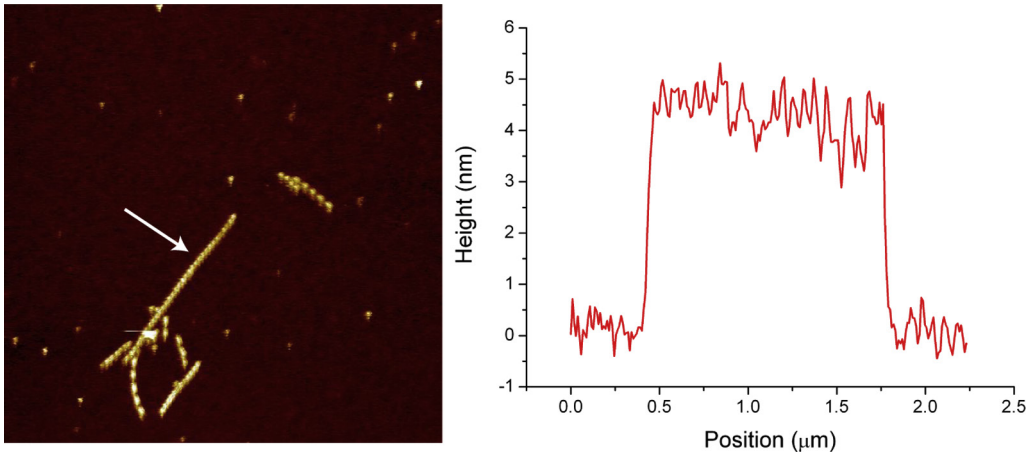

FIGURE 29.9 Typical AFM image of wild-type fibrils on a POPC–POPG-supported bilayer with corresponding height profile of the fibril indicated with an arrow. Image size is 5×5 μm, and the z-range is 10 nm.

2D equilibration is fulfilled. The question we set out to address is whether this situation also holds for deposition on mica. If this mode of fibril deposition is also valid for deposition on mica, the apparent persistence lengths would be the same, as we can see for the wild-type and E46K. However, if aS fibrils were to be irreversibly trapped onto the mica surface, the apparent persistence length would be lower than that compared to the 2D equilibrated situation. The opposite has been observed for the mutant A30P and A53T fibrils.

One possible explanation for the lower apparent persistence of fibrils deposited on POPC may be the fact that they are still able to move during scanning, as has been shown earlier (Fig. 29.2). As the fibril is moving during scanning, the AFM image of the fibril is slightly deformed. It is not very straightforward to see what influence this image deformation has on the persistence length, but because the fibrils appear as relatively stiff features (as compared to DNA, which is much more flexible), it is likely that the movement of the fibril will introduce larger curvatures in the deformed contour, when compared to a non-moving fibril. This will offset the persistence length to lower values. In connection with this argument, it is noteworthy to mention the correlation between the affinity of the fibrils to the surface and the difference in persistence length when fibrils deposited on mica and POPC are compared. Both A53T and A30P fibrils have a lower affinity for the POPC layer when compared to the other mutants, and are, for that reason, expected to be more mobile, which then leads to a slight underestimation of the persistence length.

In conclusion, because the persistence lengths of most of the deposited fibrils on either mica or POPC are comparable, we can conclude that there is no trapping effect for aS fibrils on mica, as we and others have hypothesized in earlier studies [44,45,48,49].

WILD-TYPE FIBRILS ON A POPC–POPG SUPPORTED BILAYER

In the previous section we described the analysis of aS fibrils deposited on POPC-supported lipid bilayers. Besides determining the morphologic characteristics of the protein fibrils, such as height, length, and periodicity in height modulation along the fibril, we have determined the flexibility expressed in terms of persistence length. POPC is zwitterionic and therefore neutrally charged under the conditions used in this study, such that the fibrils are expected to be only weakly bound to the bilayer. In a cellular environment membranes are not simply composed of neutral phospholipids, but of mixtures of many lipids, of which a certain fraction are anionic lipids. To explore the interactions of aS fibrils to more native membranes, which are partly negatively charged, we have deposited wild-type aS fibrils on a mixture of POPC and POPG.

Wild-type aS fibrils showed similar affinity for the POPC–POPG bilayer as compared to the POPC-only bilayer. Analysis of 20 images of POPC–POPG bilayers showed the presence of 31 bound fibrils, compared to 76 bound fibrils in 40 images for the POPC membrane. However, no fibril movement was observed on the POPC–POPG surface, which could indicate a different, most likely stronger, interaction. The average height of the fibrils on this mixed bilayer is 5.1 ± 1.5 nm (N = 31), which is considerably lower than the height obtained on mica (9.3 nm) and POPC (8.4 nm) surfaces. A typical height image of wild-type fibrils on a POPC–POPG membrane is shown in Figure 29.9, including a line section, clearly showing the reduced height of the fibrils. This reduced apparent fibril height on the mixed POPC–POPG bilayer could imply that the fibrils are incorporated in the core of the membrane.

On the POPC–POPG bilayer the fibrils were significantly lower in height (more than 3 nm) when compared

to the fibrils on the POPC bilayer. Compared to the fibrils on POPC there was almost no movement of the fibrils on the POPC–POPG membrane. This observation combined with the reduced fibril height suggests that the fibrils are incorporated in the membrane core. Previously, fibrils were found to be disruptive to POPG-only vesicles. Incorporation of fibrils in the membrane, thereby thinning the thickness of the hydrophobic core, could be the reason for this vesicle disruption [50]. Due to the strong interaction between the fibril and the lipids constituting the membrane, one can imagine that this induces a reorganization of the lipids in the bilayer leading to membrane thinning and even disruption. Additionally, the lack of movement of the fibrils on the membrane indicates that the lipids interacting with the fibrils do not diffuse freely any more. Presumably, the local enrichment of POPG and its interaction with fibrils leads to the formation of solid lipid domains, which also may impair the membrane's integrity.

CONCLUSIONS

We have evaluated the effect of the supporting substrate on quantitative measures of amyloid fibril morphologies imaged with atomic force microscopy. We report a systematic morphologic and mechanical analysis of four different aS variants (wild-type, E46K, A53T and A30P) on various hard surfaces and supported lipid bilayers. Although the monomeric form of the protein does not bind to the POPC membrane, the fibrils do show affinity – but do not seem to be incorporated within the membrane. On POPG–POPC mixed membranes the fibrils do seem to be incorporated, as can be inferred from their reduced height and lack of movement on this mixed-lipid bilayer. These findings suggest that the fibrils partially embed into the lipid bilayer, thereby locally reorganizing the lipids, which could impair membrane integrity.

The ability of the fibrils to move around on the POPC membrane gave the opportunity to investigate unequivocally the persistence lengths of the aS fibrils (3.3 to 7.1 μm) without relying on any assumption on whether the fibrils are adsorbed in a thermal equilibrium state. This also made it possible to compare the persistence length values measured on mica to see whether the equilibrium assumption holds for mica surfaces. When comparing the persistence length of the fibrils obtained on the membranes with those on deposited on mica, we can conclude that there is no trapping effect for aS fibrils on mica.

MATERIALS AND METHODS

α-Synuclein and Fibril Preparation

Recombinant expression and purification of wild-type, E46K, A30P and A53T variant aS protein was performed as described previously [27]. To produce fibrils, 250 μM monomeric wild-type, E46K, A53T and A30P aS solutions in 10 mM Tris-HCl, pH 7.4, were incubated at 70°C in tubes under constant shaking for 24 hours.

Sample Preparation

For AFM imaging of protein structures on mica, the sample preparation was performed by placing 4 μl of a 20-times diluted protein solution on freshly cleaved mica and allowing it to adsorb for 2 minutes. The sample was washed gently with 200 μl MilliQ water and dried carefully under a gentle stream of nitrogen gas. For imaging in liquid, the sample was washed with 200 μl of fresh buffer (10 mM Tris-HCl and 50 mM NaCl) and was not allowed to dry.

Atomic Force Microscopy

Tapping-mode AFM imaging in a liquid environment was performed on Bioscope Catalyst (Bruker, Santa Barbara CA, USA). All measurements were made with an MSCT silicon nitride probe (MSCT, tip F, k = 0.6 N/m, 10 nm nominal tip radius (Bruker, Santa Barbara CA, USA)). Imaging was performed in tapping mode with low force settings (80–90% of the free amplitude) to minimize interaction with the sample. The free amplitude in liquid was 2–3 nm compared to 100 nm in ambient air. The force settings during imaging on the fluid lipid membranes were even lower (95–98% of the free amplitude).

REFERENCES

[1] Breydo L, Wu JW, Uversky VN. α-Synuclein misfolding and Parkinson's disease. Biochimica Biophysica Acta 2012;1822:261–85.
[2] Goedert M. Alpha-synuclein and neurodegenerative diseases. Nat Rev Neurosci 2001;2:492–501.
[3] Cabin DE, Shimazu K, Murphy D, Cole NB, Gottschalk W, McIlwain KL, et al. Synaptic vesicle depletion correlates with attenuated synaptic responses to prolonged repetitive stimulation in mice lacking alpha-synuclein. J Neurosci 2002;22:8797–807.
[4] Chandra S, Gallardo G, Fernandez-Chacon R, Schluter OM, Sudhof TC. Alpha-synuclein cooperates with CSPalpha in preventing neurodegeneration. Cell 2005;123:383–96.
[5] Murphy DD, Rueter SM, Trojanowski JQ, Lee VM. Synucleins are developmentally expressed, and alpha-synuclein regulates the size of the presynaptic vesicular pool in primary hippocampal neurons. J Neurosci 2000;20:3214–20.
[6] Kruger R, Kuhn W, Muller T, Woitalla D, Graeber M, Kosel S, et al. Ala30Pro mutation in the gene encoding alpha-synuclein in Parkinson's disease. Nat Genet 1998;18:106–8.
[7] Zarranz JJ, Alegre J, Gomez-Esteban JC, Lezcano E, Ros R, Ampuero I, et al. The new mutation, E46K, of alpha-synuclein causes Parkinson and Lewy body dementia. Ann Neurol 2004;55:164–73.
[8] Polymeropoulos MH, Lavedan C, Leroy E, Ide SE, Dehejia A, Dutra A, et al. Mutation in the alpha-synuclein gene identified in families with Parkinson's disease. Science 1997;276:2045–7.

[9] Choi W, Zibaee S, Jakes R, Serpell LC, Davletov B, Crowther RA, et al. Mutation E46K increases phospholipid binding and assembly into filaments of human alpha-synuclein. FEBS Lett 2004;576:363–8.
[10] Fredenburg RA, Rospigliosi C, Meray RK, Kessler JC, Lashuel HA, Eliezer D, et al. The impact of the E46K mutation on the properties of alpha-synuclein in its monomeric and oligomeric states. Biochemistry 2007;46:7107–18.
[11] Li J, Uversky VN, Fink AL. Effect of familial Parkinson's disease point mutations A30P and A53T on the structural properties, aggregation, and fibrillation of human alpha-synuclein. Biochemistry 2001;40:11604–13.
[12] Pandey N, Schmidt RE, Galvin JE. The alpha-synuclein mutation E46K promotes aggregation in cultured cells. Exp Neurol 2006;197:515–20.
[13] Smith DP, Tew DJ, Hill AF, Bottomley SP, Masters CL, Barnham KJ, et al. Formation of a high affinity lipid-binding intermediate during the early aggregation phase of alpha-synuclein. Biochemistry 2008;47:1425–34.
[14] Georgieva ER, Ramlall TF, Borbat PP, Freed JH, Eliezer D. The lipid-binding domain of wild type and mutant alpha-synuclein: compactness and interconversion between the broken and extended helix forms. J Biol Chem 2010;285:28261–74.
[15] Jo E, Fuller N, Rand RP, St George-Hyslop P, Fraser PE. Defective membrane interactions of familial Parkinson's disease mutant A30P alpha-synuclein. J Mol Biol 2002;315:799–807.
[16] Stöckl M, Fischer P, Wanker E, Herrmann A. Alpha-synuclein selectively binds to anionic phospholipids embedded in liquid-disordered domains. J Mol Biol 2008;375:1394–404.
[17] Ulmer TS, Bax A. Comparison of structure and dynamics of micelle-bound human alpha-synuclein and Parkinson disease variants. J Biol Chem 2005;280:43179–87.
[18] Serpell LC, Berriman J, Jakes R, Goedert M, Crowther RA. Fiber diffraction of synthetic alpha-synuclein filaments shows amyloid-like cross-beta conformation. Proc Natl Acad Sci USA 2000;97:4897–902.
[19] Vilar M, Chou HT, Luhrs T, Maji SK, Riek-Loher D, Verel R, et al. The fold of alpha-synuclein fibrils. Proc Natl Acad Sci USA 2008;105:8637–42.
[20] Forster E, Lewy FH. Paralysis Agitans. Berlin: Springer Verlag; 1912.
[21] Ohama E, Ikuta F. Parkinson's disease: distribution of Lewy bodies and monoamine neuron system. Acta Neuropathol 1976;34:311–9.
[22] Shults CW. Lewy bodies. Proc Natl Acad Sci USA 2006;103:1661–8.
[23] Spillantini MG, Schmidt ML, Lee VM, Trojanowski JQ, Jakes R, Goedert M. Alpha-synuclein in Lewy bodies. Nature 1997;388:839–40.
[24] Bemporad F, Chiti F. Protein misfolded oligomers: experimental approaches, mechanism of formation, and structure–toxicity relationships. Chem Biol 2012;19:315–27.
[25] Winner B, Jappelli R, Maji SK, Desplats PA, Boyer L, Aigner S, et al. In vivo demonstration that α-synuclein oligomers are toxic. Proc Natl Acad Sci USA 2011;108:4194–9.
[26] Segers-Nolten I, van der Werf K, van Raaij M, Subramaniam V. Quantitative characterization of protein nanostructures using atomic force microscopy. Conf Proc IEEE Eng Med Biol Soc 2007;2007:6609–12.
[27] van Raaij ME, Segers-Nolten IM, Subramaniam V. Quantitative morphological analysis reveals ultrastructural diversity of amyloid fibrils from alpha-synuclein mutants. Biophys J 2006;91:L96–98.
[28] Jansen R, Dzwolak W, Winter R. Amyloidogenic self-assembly of insulin aggregates probed by high resolution atomic force microscopy. Biophys J 2005;88:1344–53.
[29] Khurana R, Ionescu-Zanetti C, Pope M, Li J, Nielson L, Ramirez-Alvarado M, et al. A general model for amyloid fibril assembly based on morphological studies using atomic force microscopy. Biophys J 2003;85:1135–44.
[30] Hoyer W, Antony T, Cherny D, Heim G, Jovin TM, Subramaniam V. Dependence of alpha-synuclein aggregate morphology on solution conditions. J Mol Biol 2002;322:383–93.
[31] Hoyer W, Cherny D, Subramaniam V, Jovin TM. Rapid self-assembly of alpha-synuclein observed by in situ atomic force microscopy. J Mol Biol 2004;340:127–39.
[32] van Noort SJT, van der Werf KO, de Grooth BG, van Hulst NF, Greve J. Height anomalies in tappingmode atomic force microscopy in air caused by adhesion. Ultramicroscopy 1997;69:117–27.
[33] Sherratt MJ, Holmes DF, Shuttleworth CA, Kielty CM. Substrate-dependent morphology of supramolecular assemblies: fibrillin and type-VI collagen microfibrils. Biophys J 2004;86:3211–22.
[34] Muller DJ, Amrein M, Engel A. Adsorption of biological molecules to a solid support for scanning probe microscopy. J Struct Biol 1997;119:172–88.
[35] van Rooijen BD, Claessens MM, Subramaniam V. Membrane binding of oligomeric alpha-synuclein depends on bilayer charge and packing. FEBS Lett 2008;582:3788–92.
[36] Rhoades E, Ramlall TF, Webb WW, Eliezer D. Quantification of alpha-synuclein binding to lipid vesicles using fluorescence correlation spectroscopy. Biophys J 2006;90:4692–700.
[37] Shvadchak VV, Falomir-Lockhart LJ, Yushchenko DA, Jovin TM. Interactions of α-synuclein with lipids and artificial membranes monitored by ESIPT probes. In: Jelinek R, editor. Lipids and Cellular Membranes in Amyloid Diseases. Weinheim: Wiley-VCH; 2011.
[38] Seu KJ, Pandey AP, Haque F, Proctor EA, Ribbe AE, Hovis JS. Effect of surface treatment on diffusion and domain formation in supported lipid bilayers. Biophys J 2007;92:2445–50.
[39] Rivetti C, Guthold M, Bustamante C. Scanning force microscopy of DNA deposited onto mica: equilibration versus kinetic trapping studied by statistical polymer chain analysis. J Mol Biol 1996;264:919–32.
[40] Paez A, Tarazona P, Mateos-Gil P, Velez M. Self-organization of curved living polymers: FtsZ protein filaments. Soft Matter 2009;5:2625–37.
[41] Sweers KKM, Bennink ML, Subramaniam V. Atomic force microscopy study of substrate influences on morphologies of α-synuclein amyloid fibrils. Proc Annu IEEE/EMBS Benelux Chapter 2009:89–92.
[42] Adamcik J, Mezzenga R. Adjustable twisting periodic pitch of amyloid fibrils. Soft Matter 2011;7:5437–43.
[43] Sweers KKM, van der Werf KO, Bennink ML, Subramaniam V. Atomic force microscopy under controlled conditions reveals structure of C-terminal region of alpha-synuclein in amyloid fibrils. ACS Nano 2012;6:5952–60.
[44] Sweers KKM, Segers-Nolten IMJ, Bennink ML, Subramaniam V. Structural model for [small alpha]-synuclein fibrils derived from high resolution imaging and nanomechanical studies using atomic force microscopy. Soft Matter 2012;8:7215–22.
[45] Smith JF, Knowles TP, Dobson CM, Macphee CE, Welland ME. Characterization of the nanoscale properties of individual amyloid fibrils. Proc Natl Acad Sci USA 2006;103:15806–11.
[46] Relini A, Torrassa S, Ferrando R, Rolandi R, Campioni S, Chiti F, et al. Detection of populations of amyloid-like protofibrils with different physical properties. Biophys J 2010;98:1277–84.

[47] Mucke N, Kreplak L, Kirmse R, Wedig T, Herrmann H, Aebi U, et al. Assessing the flexibility of intermediate filaments by atomic force microscopy. J Mol Biol 2004;335:1241–50.

[48] Knowles TP, Fitzpatrick AW, Meehan S, Mott HR, Vendruscolo M, Dobson CM, et al. Role of intermolecular forces in defining material properties of protein nanofibrils. Science 2007;318:1900–3.

[49] Wang JC, Turner MS, Agarwal G, Kwong S, Josephs R, Ferrone FA, et al. Micromechanics of isolated sickle cell hemoglobin fibers: bending moduli and persistence lengths. J Mol Biol 2002;315:601–12.

[50] Kayed R, Sokolov Y, Edmonds B, McIntire TM, Milton SC, Hall JE, et al. Permeabilization of lipid bilayers is a common conformation-dependent activity of soluble amyloid oligomers in protein misfolding diseases. J Biol Chem 2004;279:46363–6.